Quantitative biokinetics of titanium dioxide nanoparticles after intratracheal instillation in rats (Part 3)

Journal:	*Nanotoxicology*
Manuscript ID	TNAN-2016-0178.R2
Manuscript Type:	Original Article
Date Submitted by the Author:	n/a
Complete List of Authors:	Kreyling, Wolfgang; Helmholtz Center Munich – German Research Center for Environmental Health, Comprehensive Pneumology Center, Institute of Lung Biology and Disease; Helmholtz Center Munich – German Research Center for Environmental Health, Institute of Epidemiology 2 Holzwarth, Uwe; Joint Research Centre, Institute for Health and Consumer Protection Hirn, Stephanie; Helmholtz Center Munich – German Research Center for Environmental Health, Comprehensive Pneumology Center, Institute of Lung Biology and Disease Kozempel, Ján; Joint Research Centre, Institute for Health and Consumer Protection Wenk, Alexander; Helmholtz Center Munich – German Research Center for Environmental Health, Comprehensive Pneumology Center, Institute of Lung Biology and Disease Haberl, Nadine; Helmholtz Center Munich – German Research Center for Environmental Health , Comprehensive Pneumology Center, Institute of Lung Biology and Disease Schleh, Carsten; Helmholtz Center Munich – German Research Center for Environmental Health, Comprehensive Pneumology Center, Institute of Lung Biology and Disease Schäffler, Martin; Helmholtz Center Munich – German Research Center for Environmental Health, Comprehensive Pneumology Center, Institute of Lung Biology and Disease Lipka, Jens; Helmholtz Center Munich – German Research Center for Environmental Health, Comprehensive Pneumology Center, Institute of Lung Biology and Disease

	Semmler-Behnke, Manuela; Helmholtz Center Munich – German Research Center for Environmental Health, Comprehensive Pneumology Center, Institute of Lung Biology and Disease Gibson, Neil; Joint Research Centre, Institute for Health and Consumer Protection
Keywords:	Size-selected, radiolabeled titanium dioxide nanoparticles, intratracheal instillation, nanoparticle translocation across the air-blood-barrier, gut-absorption of swallowed nanoparticles, accumulation in secondary organs and tissues
Abstract:	The biokinetics of a size-selected fraction (70nm median size) of commercially available and 48V-radiolabeled [48V]TiO2 nanoparticles has been investigated in healthy adult female Wistar-Kyoto rats at retention time-points of 1h, 4h, 24h, 7d and 28d after intratracheal instillation of a single dose of an aqueous [48V]TiO2-nanoparticle suspension. A completely balanced quantitative biodistribution in all organs and tissues was obtained by applying typical [48V]TiO2-nanoparticle doses in the range of 40-240 μg•kg-1 bodyweight and making use of the high sensitivity of the radiotracer technique. The [48V]TiO2-nanoparticle content was corrected for residual blood retained in organs and tissues after exsanguination and for 48V-ions not bound to TiO2-nanoparticles. About 4% of the initial peripheral lung dose passed through the air-blood-barrier after 1h and were retained mainly in the carcass (4%); 0.3% after 28d. Highest organ fractions of [48V]TiO2-nanoparticles present in liver and kidneys remained constant (0.03%). [48V]TiO2-nanoparticles which entered across the gut epithelium following fast and long-term clearance from the lungs via larynx increased from 5-20% of all translocated/absorbed [48V]TiO2-nanoparticles. This contribution may account for 1/5 of the nanoparticle retention in some organs. After normalizing the fractions of retained [48V]TiO2-nanoparticles to the fraction that reached systemic circulation, the biodistribution was compared with the biodistributions determined after IV-injection (Part-1) and gavage (Part-2). The biokinetics patterns after IT-instillation and gavage were similar but both were distinctly different from the pattern after intravenous injection disproving the latter to be a suitable surrogate of the former applications. Considering that chronic occupational inhalation of relatively biopersistent TiO2-particles (including nanoparticles) and accumulation in secondary organs may pose long-term health risks, this issue should be scrutinized more comprehensively.

Quantitative biokinetics of titanium dioxide nanoparticles after intratracheal instillation in rats (Part 3)

Wolfgang G. Kreyling[§*#], Uwe Holzwarth[+], Nadine Haberl*, Jan Kozempel[+1], Alexander Wenk*[2], Stephanie Hirn*, Carsten Schleh*[3], Martin Schäffler*, Jens Lipka*, Manuela Semmler-Behnke*[4] and Neil Gibson[+]

* Helmholtz Center Munich – German Research Center for Environmental Health, Comprehensive Pneumology Center, Institute of Lung Biology and Disease, Helmholtz Centre Munich, Ingolstaedter Landstrasse 1, D-85764 Neuherberg / Munich, Germany,

[#] Helmholtz Center Munich – German Research Center for Environmental Health, Institute of Epidemiology 2, Ingolstaedter Landstrasse 1, D-85764 Neuherberg / Munich, Germany

[+] European Commission, Joint Research Centre, Directorate F – Health, Consumers and Reference Materials, Via E. Fermi 2749, I-21027 Ispra (VA), Italy

[§] Corresponding author
Wolfgang G. Kreyling
Institute of Epidemiology 2
Helmholtz Center Munich,
Ingolstaedter Landstrasse 1
D-85764 Neuherberg / Munich
Germany
Phone: +49 89 2351 4817
E-mail address: Kreyling@helmholtz-muenchen.de

[1] Current address: Czech Technical University in Prague, Faculty of Nuclear Sciences and Physical Engineering, Břehová 7, CZ-11519 Prague 1, Czech Republic
[2] Current address: Dept. Infrastructure, Safety, Occupational Protection, German Research Center for Environmental Health, D-85764 Neuherberg / Munich, Germany
[3] Current address: Abteilung Gesundheitsschutz, Berufsgenossenschaft Holz und Metall, D-81241 München, Germany
[4] Current address: Bavarian Health and Food Safety Authority, D-85764Oberschleissheim, Germany

Keywords

Size-selected, radiolabeled titanium dioxide nanoparticles; intratracheal instillation; nanoparticle translocation across the air-blood-barrier; gut-absorption of swallowed nanoparticles; accumulation in secondary organs and tissues; different biokinetics patterns after intratracheal instillation and gavage versus intravenous injection

Abstract

The biokinetics of a size-selected fraction (70nm median size) of commercially available and ^{48}V-radiolabeled [^{48}V]TiO_2 nanoparticles has been investigated in healthy adult female Wistar-Kyoto rats at retention time-points of 1h, 4h, 24h, 7d and 28d after intratracheal instillation of a single dose of an aqueous [^{48}V]TiO_2-nanoparticle suspension. A completely balanced quantitative biodistribution in all organs and tissues was obtained by applying typical [^{48}V]TiO_2-nanoparticle doses in the range of 40-240 $\mu g \cdot kg^{-1}$ bodyweight and making use of the high sensitivity of the radiotracer technique.

The [^{48}V]TiO_2-nanoparticle content was corrected for residual blood retained in organs and tissues after exsanguination and for ^{48}V-ions not bound to TiO_2-nanoparticles. About 4% of the initial peripheral lung dose passed through the air-blood-barrier after 1h and were retained mainly in the carcass (4%); 0.3% after 28d. Highest organ fractions of [^{48}V]TiO_2-nanoparticles present in liver and kidneys remained constant (0.03%). [^{48}V]TiO_2-nanoparticles which entered across the gut epithelium following fast and long-term clearance from the lungs via larynx increased from 5-20% of all translocated/absorbed [^{48}V]TiO_2-nanoparticles. This contribution may account for 1/5 of the nanoparticle retention in some organs.

After normalizing the fractions of retained [^{48}V]TiO_2-nanoparticles to the fraction that reached systemic circulation, the biodistribution was compared with the biodistributions determined after IV-injection (Part-1) and gavage (Part-2). The biokinetics patterns after IT-instillation and gavage were similar but both were distinctly different from the pattern after intravenous injection disproving the latter to be a suitable surrogate of the former applications. Considering that chronic occupational inhalation of relatively biopersistent TiO_2-particles (including nanoparticles) and accumulation in secondary organs may pose long-term health risks, this issue should be scrutinized more comprehensively.

Introduction

Part 1 and 2 of this series of biokinetics studies (Kreyling, submitted-a, Kreyling, submitted-b) dealt with intravenously injected and intra-esophageally instilled (gavage) TiO_2 nanoparticles (TiO_2NP), respectively. The background for our interest in TiO_2NP, based on by their continuously expanding application spectrum in consumer products, as food additives and in the biomedical field (Christensen, 2011) was expounded there. The present work investigates the biokinetics of TiO_2 nanoparticles after intratracheal instillation since inhalation during manufacturing and handling is the main exposure route for occupationally exposed subjects (Christensen, 2011). Despite the rapid rise in use of TiO_2NP little is still known about the health risks related to occupational exposure. Based on the experimental evidence from animal inhalation studies TiO_2 nanoparticles have been classified as "possibly carcinogenic to humans" (Baan, 2007, Echa-Corap, 2016, Niosh, 2011).

For the public the average daily oral dose of TiO_2-particles exceeds the daily inhaled and deposited TiO_2 particle dose by at least two orders of magnitude since public ambient particle concentrations have been reported up to 50 $\mu g \cdot m^{-3}$, while occupational TiO_2-particle concentrations may reach currently established limits of 5 $mg \cdot m^{-3}$ (Shi, 2013). Hence, with a daily inhaled air volume of 20 m^3 and a deposited fraction of 30% in the lungs (Geiser, 2010) the daily deposited lung dose can vary between 0.3 $mg \cdot d^{-1}$ for a member of the public up to 10 $mg \cdot d^{-1}$ for an exposed worker (8h of exposure), which translates into doses of 4.3 $\mu g \cdot kg^{-1}$ BW to 143 $\mu g \cdot kg^{-1}$ BW for an adult with 70 kg bodyweight (BW).

In vivo and *in vitro* studies describing toxic effects in the lungs were recently reviewed by (Shi, 2013). An early key inhalation study demonstrated that nano-sized TiO_2-particles can cross the air-blood-barrier (ABB) to a greater extent and cause more inflammation in rat lungs than exposure to the same airborne mass concentration of larger, submicron TiO_2-particles (Ferin, 1992). This report was the first to show that an inhaled TiO_2-material with low toxicity in the form of submicron particles could be toxic in the form of nano-sized particles.

Recently, the same group has examined the effect of dose-rate on acute respiratory tract inflammation when exposing rats to an equivalent dose of deposited TiO_2NP by IT-instillation and whole body inhalation. They conclude that high dose-rate delivery elicits significantly greater inflammation compared to low dose-rate delivery (Baisch, 2014).

With the present biokinetics study, using intratracheal instillation (IT) of identical ^{48}V-radiolabeled [^{48}V]TiO_2NP that were simultaneously applied by intravenous injection and gavage, it is possible to compare the biokinetics of [^{48}V]TiO_2NP translocated through the ABB with those that crossed the intestinal epithelium and those that directly reached systemic circulation by intravenous injection.

The comparative study of [^{48}V]TiO_2NP clearance from blood to secondary organs and tissues was designed to investigate possible differences in the biokinetic fate after the three exposure routes and to gain information on the role of mononucleated-phagocytic cells in blood, organs and tissues. Since we knew from previous biokinetics studies on a suite of monodisperse gold nanoparticles (AuNP) administered *via* the same three routes (Kreyling, 2011, Hirn, 2011, Kreyling, 2014, Schleh, 2012) and after inhalation of 20 nm iridium nanoparticles (IrNP) (Kreyling, 2002, Semmler, 2004, Semmler-Behnke, 2007) or 20 nm elemental carbon nanoparticles (ECNP) (Kreyling, 2009), that the accumulation dynamics occurs rather rapidly during the first 24-hours we chose three time-points of investigation – 1h, 4h, 24h – to study the rapid accumulation dynamics observed previously, followed by two time-points at 7d and 28d in order to assess possible slower processes of accumulation, redistribution and clearance. For this purpose, retained [^{48}V]TiO_2NP doses in different organs of interest, selected tissues and body fluids were determined, including the carcass and the entire fecal and urinary excretions of each animal to provide a complete balance of the fate of the applied [^{48}V]TiO_2NP in the entire organism.

Materials and Methods

Radiolabeling, suspension and size selection of TiO_2NP

Two batches of 20 mg ST-01 TiO_2NP were irradiated with a proton beam current of 5 μA using a cyclotron (cf. Supplementary Material (SI-IT)). One, with a ^{48}V-activity concentration of 1.0 MBq•mg^{-1} (^{48}V-activity per TiO_2NP mass), was used for the 1h, 4h and 24h retention experiments. The second one was irradiated on five consecutive days, yielding an ^{48}V-activity concentration of 2.35 MBq•mg^{-1} and was used for the 7d and 28d retention experiments. The atomic ratio of ^{48}V:Ti in the nanoparticles is about $2.6•10^{-7}$ and $6.2•10^{-7}$, respectively. Since proton irradiation and the chemical difference of the radiolabel, may result in a non-perfect integration of the ^{48}V in the TiO_2 matrix the [^{48}V]TiO_2NP were washed to remove ^{48}V ions (SI-IT).

Size selection was performed in a repeated sequence of nanoparticle suspension, ultrasound homogenization, washing by centrifugation and re-suspension in order to remove excess sodium pyrophosphate, used as a surfactant, to eliminate larger aggregates/agglomerates and to minimize the content of free ionic ^{48}V as detailed in theSI-IT. The final size-selected and radiolabeled, nano-sized aggregates/agglomerates of [^{48}V]TiO_2NP were suspended in water.

For each retention time-point to be studied a new batch of size-selected [^{48}V]TiO_2NP was prepared, characterized and immediately applied to four rats for each exposure path, *i.e.*, intravenously (IV), by gavage (GAV) and by intratracheal (IT) instillation, which improves the comparability of the results as the studies were started with the same nanoparticle properties.

Characterization of nanoparticles

The hydrodynamic diameter and the zeta potential of the size selected [^{48}V]TiO_2NP were measured in triplicates several times during the size-selection process for control purposes and prior to application using dynamic-light-scattering (DLS; Malvern Zetasizer, Herrenberg, Germany). Samples for transmission-electron-microscopy were prepared from the aqueous suspensions on glow discharged 300 mesh Formvar®-coated copper grids and investigated with a Philips 300 TEM at 60 kV acceleration voltage.

Experimental procedures – Study design

The biokinetics of [^{48}V]TiO_2NP was studied at five retention time-points 1h, 4h, 24h, 7d and 28d after IT-instillation in four rats for each retention time-point as sketched below:

Study	IT-instillation, 0h	dissection time-points for biodistribution analyses				
MAIN	[^{48}V]TiO_2NP	1h	4h	24h	7d	28d
AUX	^{48}V ions			24h	7d	

Immediately after the final preparation step the [^{48}V]TiO_2NP suspensions were applied in a single bolus of about 10 µg of [^{48}V]TiO_2NP per rat. The time-points at 7d and 28d were studied with higher doses (20-60 µg) in order to preserve sufficient sensitivity in spite of longer radioactive decay and to detect any minor redistribution and clearing processes.

In order to investigate the absorption and biodistribution of soluble, ionic ^{48}V an auxiliary study was performed at 24h and 7d after intratracheal instillation with the purpose of correcting the biodistributions of [^{48}V]TiO_2NP for contributions of ^{48}V-ions possibly released from the [^{48}V]TiO_2NP. In order to mimic ^{48}V released by [^{48}V]TiO_2NP 0.33 µg•µL^{-1} ionic $Ti(NO_3)_4$ was added to carrier-free ionic ^{48}V. The pH value was adjusted to 5. For the experiments 60 µL of solution containing 27 kBq ionic ^{48}V and 20 µg of ionic Ti were administered per rat. Based on the biodistribution of ^{48}V-ions and the urinary excretion

kinetics after intratracheal instillation of ^{48}V-ions and of [^{48}V]TiO_2NP the biodistribution of [^{48}V]TiO_2NP was corrected for contributions of ^{48}V-ions according to the mathematical procedure derived in theSI-IT.

Animals

Healthy, female Wistar-Kyoto rats (Janvier, Le Genest Saint Isle, France), 8–10 weeks of age (267.0±9.2 g, mean (±SD) body weight) were housed in pairs in relative-humidity and temperature-controlled ventilated cages on a 12h day/night cycle. Rodent diet and water were provided *ad libitum*. After purchase, the rats were adapted for at least two weeks and then randomly attributed to the experimental groups. All experiments were conducted under German federal guidelines for the use and care of laboratory animals and were approved by the Regierung von Oberbayern (Government of District of Upper Bavaria, Approval No. 211-2531-94/04) and by the Institutional Animal Care and Use Committee of Helmholtz Centre Munich.

[^{48}V]TiO_2NP suspensions were applied in a single bolus immediately after preparation to non-fasted animals by IT-instillation (SI-IT), and the animals were kept individually in metabolic cages for quantitative collection of excretions. At 1h, 4h, 24h, 7d and 28d after intratracheal instillation, rats were anesthetized and euthanized by exsanguination *via* the abdominal aorta.

Sample preparation, radiometric analysis

The syringes and catheters used for intratracheal instillation were collected after use in order to quantify [^{48}V]TiO_2NP retained therein.

For γ-ray spectrometry, all organs, tissues and excretions were collected and ^{48}V-radioactivities were measured without any further physico-chemical processing (Kreyling, 2011, Hirn, 2011, Kreyling, 2014, Schleh, 2012) to obtain quantitative, fully balanced

biodistributions. Since by exsanguination only about (60-70)% of the blood volume could be recovered the residual blood contents of organs and tissues were calculated according to (Oeff, 1955) and the ^{48}V-radioactivities of the organs were adjusted accordingly (seeSI-IT).

The ^{48}V-radioactivity of the samples was measured by γ-ray spectrometry using shielded NaI detectors properly calibrated in γ-ray energy and detection efficiency for the 511keV-radiation created by ^{48}V decay. Samples yielding background-corrected counts in the 511keV region-of-interest of the ^{48}V γ-ray spectrum were considered below the detection limit (DL; < 0.2 Bq) when the number of counts was less than three standard deviations of the background counts.

Data evaluation

[^{48}V]TiO_2NP accumulation and retention is based on two specific clearance pathways, (i) [^{48}V]TiO_2NP translocation across the ABB into blood circulation and (ii) [^{48}V]TiO_2NP absorption across the GIT walls of [^{48}V]TiO_2NP which were eliminated from the lungs towards the larynx and swallowed into the GIT. The latter pathway has a fast component for those [^{48}V]TiO_2NP deposited on the conducting airways that are rapidly cleared by mucociliary action (MCC) followed by a slow component for [^{48}V]TiO_2NP in the peripheral lungs which are transported by alveolar macrophages (AM).

Nanoparticles rapidly eliminated from the lungs by MCC are not available for translocation through the ABB. Therefore, all data describing nanoparticle translocation through the ABB were normalized to the *initial peripheral lung dose* (IPLD) obtained by subtracting the ^{48}V-activity due to MCC from the IT-instilled nanoparticle dose. As outlined in theSI-IT (Eqn (S10)) the MCC fraction was estimated as the activity measured in the head (without brain), the trachea and major bronchi, the gastro-intestinal tract up to 24h and feces up to 48h.

The uptake and biodistribution of [^{48}V]TiO_2NP absorbed through the GIT was estimated using the absorption and biodistribution data from the gavage study (Kreyling, submitted-b).

For this purpose the rapidly cleared [^{48}V]TiO_2NP fraction swallowed into the GIT (MCC) followed by the long-term macrophage-mediated cleared [^{48}V]TiO_2NP fraction (LT-MC), reconstructed from fecal excretion for the various retention time-points (seeSI-IT), were considered.

Throughout this report, the determined background and decay-corrected ^{48}V-activity values of organs, tissues, blood or excretions are given as %-fractions of the IPLD, determined as the sum of all samples prepared from each animal, including its total urinary and fecal excretion, subtracting fast MCC cleared [^{48}V]TiO_2NP in each animal as described in theSI-IT. These %-fractions are averaged over four of rats in each group and are given with the standard-error-of-the-mean (SEM). The raw data of the ^{48}V-activity were corrected (i) for the residual blood content in organs or tissues after exsanguination and (ii) for the ^{48}V-activity contribution of free ^{48}V ions according to the methododlogy presented in theSI-IT.

[^{48}V]TiO_2NP concentrations, given as % IPLD•g^{-1}, were translated into nanoparticle mass per weight of organ or tissue dividing the data by the ^{48}V-activity concentration (1.0 MBq•mg^{-1} (1h, 4h, 24h) and 2.35 MBq•mg^{-1} (7d and 28d)).

All calculated significances are based on the One-Way-ANOVA test and the *post hoc* Bonferoni test. For direct comparisons between two groups, the unpaired t-test was used. $p \leq 0.05$ was considered significant.

Results

Physicochemical properties of [^{48}V]TiO_2NP

The size distributions of the size-selected [^{48}V]TiO_2NP determined by DLS are presented in Figure 1 and indicate a good reproducibility of the size selection procedure. The Z-averages (Table 1) are in a narrow range of 88 ± 11 nm, and the PDI values 0.18 ± 0.04 indicate polydisperse but rather narrow size-distributions. TEM investigations immediately after size

selection and dispersion (Figure 2) revealed approximately spherical aggregated/agglomerated entities of roughly 50 nm in diameter, made up of smaller primary particles.

With the ^{48}V-activity concentrations determined after proton irradiation the ^{48}V-activity values can be converted to [^{48}V]TiO_2NP mass. The effectively applied ^{48}V-activities and corresponding masses of [^{48}V]TiO_2NP compiled in Table 1 take into account that a fraction of the ^{48}V-activity loaded into the syringes was retained there.

Insert Table 1, Figures 1+2 here.

Fast [^{48}V]TiO_2NP clearance from airways and long-term macrophage-mediated nanoparticle clearance (LT-MC) from the lungs

A fraction of IT-instilled [^{48}V]TiO_2NP is deposited on airway epithelia, from where it is cleared rapidly within 24h towards the larynx and swallowed into the GIT. This fast mucociliary cleared (MCC) [^{48}V]TiO_2NP fraction varies considerably between individual rats, giving rise the large uncertainty shown in Table 2, even though the instillation procedure was standardized by (a) instillation by only one operator for the entire study, (b) reproducible position of the rat on a 60°-tilted board, (c) controlling breathing flow through the intratracheal catheter (excluding catheter misplacement) using a pneumotachograph, (d) IT-instillation synchronized during inhalation, (e) pushing 0.3–0.4 mL of air behind the instilled [^{48}V]TiO_2NP suspension for enhanced instillation into the peripheral lungs.

After 7 days the slow [^{48}V]TiO_2NP LT-MC clearance had become higher than the expected fraction of 14-17% based on a fractional clearance rate of 0.02–0.03 d^{-1} of the contemporary total lung dose as previously determined (Kreyling, 1990, Semmler, 2004). This deviation may have been caused by a delayed passage of MCC-cleared [^{48}V]TiO_2NP from the airways through the GIT lasting sometimes into the third day after instillation. Assuming a LT-MC-

rate of 0.02–0.03 d^{-1} an integral clearance fraction of 40-50% should be expected after 28 days, which is higher than the observed 30.5 % (Table 2).

Determination of the initial peripheral lung dose (IPLD)

The effectively applied [^{48}V]TiO_2NP dose was determined as sum of the ^{48}V-activities in all collected organs and tissues, including all excretions, determined by γ-ray spectrometry. In the present case the lungs contributed three specimens, (i) the lungs after broncho-alveolar lavage (BAL), the cells (BALC) separated from the liquid used for lung lavage by centrifugation and the fluid (BALF) phase itself.

In order to determine the fraction of the [^{48}V]TiO_2NP dose that crosses the ABB the fraction of [^{48}V]TiO_2NP that are rapidly eliminated from the lungs by mucociliary clearance (MCC) must be subtracted from the intratracheally instilled dose. The result is the initial peripheral lung dose (ILPD) which is the reference for ABB-translocation.

[^{48}V]TiO_2NP- retention in lungs and broncho-alveolar lavage

After IT-instillation the most prominent [^{48}V]TiO_2NP fraction was found in the lavaged lungs, followed by BALC and early-on in BALF. The increase of [^{48}V]TiO_2NP retention in the lavaged lungs from 43% (1h) to 68% (24h) indicates a nanoparticle relocation towards non-lavageable sites; i.e,. increased [^{48}V]TiO_2NP uptake by cells of the epithelial membrane. Figure 3A shows a high but decreasing fraction of [^{48}V]TiO_2NP in the lavaged lungs from 7d (32%) to 28d (19%). The [^{48}V]TiO_2NP fraction in BALC exhibited a pronounced increase from 23% (1h) to 40% (4h) and decreased continuously to 16% (28d), while the [^{48}V]TiO_2NP fraction in BALF decreased continuously from 31% (1h) to 0.7% (28d).

The kinetics of total [^{48}V]TiO_2NP translocation across the ABB is shown in Figure 3B. After an initial fast uptake of 4.3% (of IPLD) it rapidly declines to about 1% (of IPLD) until 4h. After 28 days still 0.4% (IPLD) is retained. This suggests rapid translocation across the ABB immediately after instillation followed by net clearance during the entire observation period. However, this does not exclude continuous translocation across the ABB and simultaneous clearance from secondary organs and tissues. The [^{48}V]TiO_2NP content in the total blood stayed between 0.1% and 0.2% during the first 24h, declined to 0.024% after 7d and further to 0.013% until 28d.

[^{48}V]TiO_2NP relocation within the lungs

[^{48}V]TiO_2NP relocation from the epithelial surface was considered for those [^{48}V]TiO_2NP which were not removed by BAL but bound and/or taken up by cells of the epithelial barrier and beyond as observed earlier {Kreyling, 2002 #943;Semmler, 2004 #952;Semmler-Behnke, 2007 #953}. Lavageable [^{48}V]TiO_2NP fractions, either associated with lavageable cells (*i.e.* alveolar macrophages (AM) in BALC or free [^{48}V]TiO_2NP in BALF) are discerned from lung retained [^{48}V]TiO_2NP fractions and are normalized to the contemporary lung dose, *i.e.*, the total amount of [^{48}V]TiO_2NP present in the lung at a certain time-point. Figure S7 (SI-IT) shows the kinetics of free [^{48}V]TiO_2NP in BALF which is about 30% of all [^{48}V]TiO_2NP in lungs 1h after IT-instillation. However, it drops very rapidly to 0.01% after 7 days. In contrast, the lavageable macrophage-associated [^{48}V]TiO_2NP account for 40% of the [^{48}V]TiO_2NP in the lungs starting from 4h until the end of the study. Accordingly, the kinetics of the estimated total number of [^{48}V]TiO_2NP in the pool of all alveolar macrophages (AM-pool) to be cleared by LT-MC is rather constant at 60% from 4h to 28d (SI-IT). Hence, about 40% of [^{48}V]TiO_2NP non-accessible to BAL-removal were relocated and retained in the epithelium and interstitium over 28 days (Kreyling, 2013).

Uptake of [^{48}V]TiO_2NP into secondary organs and tissues

Table 3 shows the [^{48}V]TiO_2NP retention of various organs and tissues as raw data (*in %IPLD*), after subtracting the contribution of ^{48}V-activity in the residual blood present in organs and tissues after exsanguination (*w/o res. Blood cont.*) and after additionally subtracting the activity attributed to free ^{48}V-ions according to the mathematical procedure derived in theSI-IT (*w/o free ^{48}V-ions*), which yielded small corrections at 1h. It can be noted that after 4h the ^{48}V-ion correction resulted in an appreciably lower [^{48}V]TiO_2NP retention in all organs and tissues. In uterus and brain no particulate ^{48}V-activity remained that could be clearly attributed to [^{48}V]TiO_2NP. The significance of the corrections was assessed by a statistical one-way ANOVA analysis and a *post-hoc* Bonferoni test. In Table 3 the corrected activity data are also presented as %IPLD/organ-mass (% IPLD·g^{-1}) and as [^{48}V]TiO_2NP mass concentrations (ng•g^{-1}). The evolution of the data sets over the various retention time-points is visualized in Figure 4.

Except for the carcass and the soft tissues none of the organs and tissues beyond the ABB reaches a total retention of 0.1% of IPLD. Liver and kidneys exhibit the highest nanoparticle burden. Against the general trend kidneys, heart and spleen showed an approximately constant or even slightly increasing retention up to 28 days. Measurable nanoparticle retention was initially (1h to 4h) also observed in the brain and uterus but fell below the detection limit after 1 day.

INSERT Table 3 and Figure 4 here

Biokinetics of [^{48}V]TiO_2NP translocated across the ABB

A comparison of the [^{48}V]TiO_2NP biokinetics after (i) IV-injection (ii) gavage and (iii) IT-instillation is hampered by the fact that IV-injected [^{48}V]TiO_2NP directly enter systemic

circulation, while only a tiny fraction of gavaged nanoparticles is absorbed through the gut walls (≈ 0.6%ID, 1h) and only a small fraction of IT-instilled nanoparticles pass the ABB (≈ 4.3%IPLD, 1h). Therefore, in the columns - IT-instillation and gavage - of Figure 5 [^{48}V]TiO_2NP percentages assigned to certain organs were normalized to the [^{48}V]TiO_2NP that reached systemic circulation (seeSI-IT). Additionally to the vastly different [^{48}V]TiO_2NP mass in systemic circulation, IV-injected [^{48}V]TiO_2NP enter the blood as a single bolus *via* the tail vein within about 10-30 seconds while [^{48}V]TiO_2NP translocation across the ABB or the GIT slows down the dose-rate by orders of magnitude at which [^{48}V]TiO_2NP reach blood circulation. Nevertheless, one hour after application [^{48}V]TiO_2NP removal from blood is more efficient leaving only 0.3%ID in blood after IV-injection while the percentage of circulating [^{48}V]TiO_2NP is tenfold higher (5% or 2%) of ABB-translocated or gut-absorbed [^{48}V]TiO_2NP, respectively, indicating very different mechanisms of removal from blood.

Insert Figure 5 here

Figure 5 shows that the retention data after IT and gavage are completely different from those after IV-injection. Most strikingly the almost 100% [^{48}V]TiO_2NP accumulation in the liver after IV-injection (Fig. 5C) is at least 10-fold higher than after ABB-translocation (Fig. 5A) or gut-absorption (Fig. 5B) over the whole observation period. The spleen values increase tenfold from 0.3% (1h) up to 3% at 28d after ABB-translocation while after IV-injection spleen values remain around 3% over the entire time; after gut-absorption the values are in the same range but with a pronounced peak after 24h. Accumulation in the lungs is rather constant after IV-injection at around 0.1% of the injected dose and at least tenfold lower than after gavage which reaches about 10% of the absorbed [^{48}V]TiO_2NP fraction at 24h and declines to 3% after 7d. Kidneys: IV-injected NP remain rather constant at 0.1%ID while ABB-translocated NP are tenfold higher increasing from 0.9-7% and gut-absorbed NP are initially <DL but increase steeply to 5% at d7. Heart: IV-injected NP remain also constant at

0.01%ID while ABB-translocated NP increase from 02-2% and gut-absorbed NP peak at 24h at 8%. Brain: IV-injected NP stay low and constant (<0.001%ID), ABB-translocated NP are <DL from 1-28 days, but gut-absorbed NP increase from 0.6-6%. Uterus: IV-injected NP stay constant at 0.01%ID, ABB-translocated NP are <DL from 1-28 days but gut-absorbed NP are <DL at 1h and about 5% later. The largest part of the translocated [^{48}V]TiO_2NP can be found in the carcass after IT-instillation and gavage (90% of the translocated nanoparticles at 1h), while after IV-injection it is only around 1% of the injected dose. In spite of the whole dose being delivered to the blood by IV-injection the dose fraction retained in the blood is tenfold lower (0.5-0.05%) than the corresponding fractions between 1-10% of translocated [^{48}V]TiO_2NP through the ABB or the GIT barrier.

[^{48}V]TiO_2NP retention originating from MCC and LT-MC and subsequent absorption across the gut walls

Since fast mucociliary [^{48}V]TiO_2NP airways clearance (MCC) and long-term macrophage-mediated clearance (LT-MC) into the GIT provide a source of [^{48}V]TiO_2NP subsequently leading to absorption of [^{48}V]TiO_2NP across the gut walls, this possible contribution to the biokinetics of intratracheally instilled nanoparticles was estimated based on the absorption data from the gavage study (Kreyling, submitted-b) as outlined in theSI-IT.

Insert Figure 6 here

Figure 6B shows that after 24h 5% of [^{48}V]TiO_2NP that reached systemic circulation were cleared from the lungs via the larynx, reached the GIT and were absorbed; however, the ratio of absorbed [^{48}V]TiO_2NP increased to 20% after 28d. This increase results from continuous LT-MC out of the lungs into the GIT followed by ongoing [^{48}V]TiO_2NP absorption while ABB translocation appears to be rather low after 24h. However, due to the initial

[^{48}V]TiO_2NP translocation across the ABB translocation dominates the accumulation in secondary organs and carcass throughout 28 days. Note, for certain retention time-points and organs of low [^{48}V]TiO_2NP accumulation – like heart and uterus - the GIT-absorbed contribution may even exceed 20%.

Discussion

For the present study a truly nano-sized nanoparticle fraction of radiolabelled, commercially available TiO_2NP was selected. The firmly radiolabeled, well characterized [^{48}V]TiO_2NP were quantified by radiometric analyses with highly sensitive γ-ray-spectrometers, which provide a dynamic radioactivity measurement range over five orders of magnitude. This enabled a completely balanced biokinetics assay. In order to determine the parenchymal [^{48}V]TiO_2NP contents in organs and tissues the [^{48}V]TiO_2NP content in the residual blood after exsanguination was subtracted.

Radiolabeling of commercially available TiO_2NP with ^{48}V by inducing nuclear reactions during proton irradiation leads to a chemical difference between radiolabel and the Ti in the surrounding matrix, which makes this approach potentially prone to ion release (Abbas, 2010, Gibson, 2011, Hildebrand, 2015, Holzwarth, 2012). Additionally, the radiolabel may be released if a slow dissolution process of the TiO_2NP was present (Vogelsberger, 2008). Since the present method detects nanoparticles *via* the presence of the ^{48}V-radiolabel a possible error caused by ^{48}V detached from nanoparticles has been estimated and corrected with the help of auxiliary biokinetics studies applying ionic ^{48}V. The importance of this correction is illustrated by the data compiled in Table 3. In brain and uterus the ^{48}V-activity detected after 24h may be entirely attributed to ions, with that of [^{48}V]TiO_2NP below the detection limit. The large corrections for free ^{48}V-ions may indicate a preferential absorption of ions through the ABB, and could be related to an increased release of ^{48}V-ions from the [^{48}V]TiO_2NP in the alveoli or after passage through the ABB.

A substantial and variable fraction of [^{48}V]TiO_2NP was retained in the application syringes and cannulas which was not observed in the auxiliary study applying ionic ^{48}V and Ti. This was most likely caused by electrostatic charge of the plastic materials used and can therefore also be expected in other investigations which did not check for retention in the application equipment, thereby causing significant dose overestimates that might explain some of the large data variability in literature.

After IT instillation [^{48}V]TiO_2NP are not only cleared out of the lungs but also relocated from the lung surface into the epithelium and interstitium (EP+IS). The rather constant 40% [^{48}V]TiO_2NP fraction relocated within EP+IS (see Fig. S7,SI-IT) can be compared to similarly constant AM-pool fractions of 80% and 20% for inhaled 20nm iridium-NP ([^{192}Ir]IrNP) and 2.1µm polystyrene particles (PSL), respectively (Lehnert, 1989, Semmler, 2004, Semmler-Behnke, 2007). In other words, [^{192}Ir]IrNP and PSL fractions of 80% and 20%, respectively, were relocated into the lung interstitium indicating a substantial biokinetics difference between nanoparticles and micron-sized particles, as discussed previously (Kreyling, 2013). The observed relocated fraction of 40% for 70nm [^{48}V]TiO_2NP is higher than that for 20nm [^{192}Ir]IrNP but lower than for micron-sized PSL, presumably due to the larger nanoparticle-size and/or material differences.

As determined earlier for [^{192}Ir]IrNP, the daily, long-term macrophage-mediated nanoparticle clearance is governed by a rate of 2-3% d^{-1} of the contemporary lung dose (Kreyling, 2002, Semmler, 2004, Semmler-Behnke, 2007). In the present study the corresponding clearance rate for [^{48}V]TiO_2NP was very similar at around 1-3 % d^{-1} (cf, Table 2). This macrophage-mediated clearance mechanism seems to be rather independent of the nanoparticle material and holds also for lung clearance of insoluble micron-sized and submicron-sized particles (Semmler, 2004) (Kreyling, 2000) (Kreyling, 1990).

Our biokinetic studies after IT-instillation confirmed TiO_2NP translocation across the ABB into the circulation leading to measurable TiO_2NP accumulations in most organs and tissues.

The largest fraction of the translocated [^{48}V]TiO_2NP was found in soft tissue followed by skeleton, which are not considered in many other biokinetic studies, while highest concentrations per organ weight were found in kidneys, liver and spleen.

Our data do not provide clear evidence on the underlying [^{48}V]TiO_2NP accumulation mechanisms. However, confronting the biokinetics data obtained for the same [^{48}V]TiO_2NP studied after IT-instillation, gavage and IV injection allows us to draw some conclusions. Most tissues and the blood itself have only a relatively low capacity for acute particle uptake *via* their mononucleated-phagocytic-system (MPS). In contrast, the liver and spleen (when considering [^{48}V]TiO_2NP mass per organ weight; Table 3) have an extraordinary high capacity *via* its MPS as reported in recent biokinetics reports (e.g. (Almeida, 2011)). Hence, following the 100-fold higher IV-injected dose, the liver collects almost all of the [^{48}V]TiO_2NP and the relatively low MPS capacities of blood and the other organs and tissues are immediately saturated. In contrast, after IT-instillation or gavage, the ABB or the gut barrier, respectively, act to greatly reduce the [^{48}V]TiO_2NP dose translocated/absorbed, and to slow the dose rate, whilst the cellular and lymphatic systems serve to further limit vascular exposure to [^{48}V]TiO_2NP.

Since biokinetics after gut-absorption was more similar to that after ABB-translocation than after IV-injection it appears that very low [^{48}V]TiO_2NP concentrations that gradually reach the circulation, affect to some extent all of the organs presumably because their MPS is not saturated at such low [^{48}V]TiO_2NP doses and translocation-rates. After lungs and carcass the liver still shows greatest uptake, perhaps consistent with its super-efficient MPS. In (Kreyling, submitted-b) we discuss the pathway of gavaged [^{48}V]TiO_2NP *via* lymphatics towards the thoracic duct of the lymph system into circulation. [^{48}V]TiO_2NP may enter the lymphatic system of the lungs *via* a similar pathway which drains to the hilar lymph-nodes and additionally to the jugular vein, and possibly also *via* mediastinal lymph-nodes towards the

thoracic duct and into circulation. In the hilar lymph-nodes at the first bifurcation and along the trachea efficient particle accumulation has been described for nanoparticles (Fromen, 2016). Therefore, we analyzed the [^{48}V]TiO_2NP content in the trachea and both main bronchi at each retention time-point. The fractions did not increase as would be expected for lymph node uptake, but decreased over time as expected for decreasing efficiency of fast and slow clearance towards the larynx leading to small [^{48}V]TiO_2NP fractions in transit through the main bronchi and trachea (SI-IT). Hence, no super-imposed lymph-node accumulation is detectable suggesting a minute contribution, and the importance of the "lymphatic" pathway remains unclear for translocated [^{48}V]TiO_2NP across the ABB. However, recent morphometric studies after inhalation of 20nm sized TiO_2NP aerosols showed TiO_2NP retention in vascular endothelial cells, indicating a pathway into circulation (Geiser, 2008, Geiser, 2005). The initially extracellular [^{48}V]TiO_2NP at low blood concentrations are likely to be taken up by circulatory MPS cells and determining the [^{48}V]TiO_2 NP fate in the organism. The [^{48}V]TiO_2NP uptake may be influenced by their protein-corona.

Similar differences were observed between 80nm-sized [^{198}Au]AuNP crossing the barriers of the lungs or gut *versus* directly IV-injected [^{198}Au]AuNP (Kreyling, 2014, Schleh, 2012, Hirn, 2011). For each administration route, the biokinetics patterns obtained from [^{198}Au]AuNP agree well with the [^{48}V]TiO_2NP data, although the comparison is limited to the first 24h due to the short ^{198}Au half-life.

The present study is limited to the level of macroscopic biokinetics and does not provide any microscopic details such as any cell-type interactions with the [^{48}V]TiO_2NP in any of the secondary organs or tissues as discussed in more detail in part 1 of this study (Kreyling, submitted). However, microscopic details were investigated in detail in two earlier studies (Geiser, 2008, Geiser, 2005) where inhaled 20nm anatase TiO_2NP aggregates/agglomerates were found in various compartments of all major cell types of the rat lung parenchyma such

as epithelial cells, macrophages, fibroblasts, capillary endothelial cells and even in erythrocytes 24h after inhalation.

Even though there is growing evidence that nanoparticles and submicron-particles can cross biological barriers, many questions concerning the role of their physico-chemical properties remain open. Additional open questions relate to the extrapolation of these rat biokinetics studies to humans; in fact, we discussed those species differences and also the considerable lack of knowledge in a previous review (Kreyling, 2013). Previously we discussed the role of the size of ^{198}Au radiolabeled nanoparticles ([^{198}Au]AuNP) ranging from 1.4nm to 200nm (Kreyling, 2014, Schleh, 2012, Hirn, 2011); the similar-sized 80nm [^{198}Au]AuNP translocate 2-3-fold less across the ABB than 70nm [^{48}V]TiO_2NP. This may be caused by the chain-aggregated *versus* spherical nanoparticle morphologies and/or by different nanoparticle materials and surface properties.

The observed [^{48}V]TiO_2NP biokinetics patterns underline the important role of MPS cells in various organs and tissues. In order to avoid the analytical difficulties of protein analyses on nanoparticle-protein-complexes *in vivo* in blood, we recently engineered covalently bound nanoparticle-protein-complexes in test tubes prior to IV-injection (Schäffler, 2014). Subsequent biokinetics studies on mice were performed using 15nm and 80nm [^{198}Au]AuNP grafted either with albumin or apo-lipoprotein-E on their surfaces. The accumulation patterns of such engineered [^{198}Au]AuNP-protein-complexes and of citrate-stabilized [^{198}Au]AuNP, on which protein-coronas formed spontaneously in blood, were found to differ by up to a factor of 100 in many secondary organs and tissues, which confirms the important role of the protein-corona on nanoparticle biokinetics.

The outer protein-shell of the nanoparticle-protein-complex leads to selected interaction/uptake in MPS cells in blood and various organs/tissues. A recent study on the stability of a “firmly” grafted polymeric shell radiolabeled with ^{111}In onto 5nm [^{198}Au]AuNP revealed that the ^{111}In distribution differed greatly from that of the [^{198}Au]AuNP. This

indicates a disintegration of the core-shell nano-structures *in vivo* and emphasizes that even grafted protein-coronas may not be as stable as anticipated (Kreyling, 2015). However, whether this finding can be explained by an exchange of proteins of a soft second protein layer formed on top of a irreversibly bound first layer as found by (Milani, 2012) for polystyrene nanoparticles, giving rise to an exposure memory effect, remains to be investigated.

The present *in vivo* study confirms earlier speculations that nanoparticles, reaching the gut following fast mucociliary clearance and long-term nanoparticle clearance *via* the larynx, may be absorbed across the gut epithelium, providing a continuous, non-negligible contribution to the accumulation of inhaled nanoparticles in secondary organs and tissues, in addition to those which had crossed the ABB. Based on the biokinetics data after gavage of the same [^{48}V]TiO_2NP this contribution was estimated quantitatively.

Conclusions

Long-term lung retention was mainly determined by macrophage-mediated clearance (LT-MC) from the alveolar region. Remarkably, about half of the TiO_2NP were similarly relocated into the interstitium and re-entrained back onto the lung-epithelium for LT-MC as previously observed for IrNP. Biokinetic studies after IT-instillation confirmed TiO_2NP translocation across the ABB into the circulation leading to small but persistent TiO_2NP accumulations in almost all studied organs and tissues. The accumulation patterns of TiO_2NP which had crossed the ABB were found to be rather similar to those TiO_2NP after absorption through the gut walls but distinctly different from the distribution pattern of directly IV-injected TiO_2NP that accumulated in secondary organs. This indicates the pivotal role of MPS cells in blood, organs and tissues whose interaction with nanoparticles may be influenced by protein-

coronas. Furthermore, we confirm that nanoparticles cleared from the lungs after IT-instillation can be absorbed in the GIT giving an additional contribution to the accumulation of nanoparticles in secondary organs and tissues.

Acknowledgements

We thank Sebastian Kaidel, Paula Mayer and Nadine Senger from the Helmholtz Center Munich for their excellent technical assistance, as well as Kamel Abbas, Antonio Bulgheroni, Giulio Cotogno, Izabela Cydzik and Federica Simonelli from the EU-Joint Research Center, who strongly supported the NP radiolabelling task.

Declaration of interest

The authors declare that they have no competing interests. The authors alone are responsible for the content and writing of the paper.

This work was partially supported by the German Research Foundation SPP 1313, the EU-FP6 project Particle-Risk (012912 (NEST)), and the EU FP7 projects NeuroNano (NMP4-SL-2008-214547), ENPRA (NMP4-SL-2009-228789) and InLIveTox (NMP-2008-1.3-2 CP-FP 228625-2) and US-NIH grant HL074022.

Supplementary Material available online

- Radiolabeling of titanium dioxide (TiO_2) nanoparticles
- Nanoparticle preparation for administration and nanoparticle characterization
- Animals
- Nanoparticle administration and animal maintenance in metabolic cages

- Sample preparation for radiometric analysis
- Radiometric and statistical analysis
- Blood correction and total blood volume
- ^{48}V activity determination of skeleton and soft tissue
- Biokinetics of soluble, ionic ^{48}V after IT-instillation
- [^{48}V]TiO_2NP accumulation and retention in secondary organs and tissues: Data evaluation and correction for release of ionic ^{48}V from [^{48}V]TiO_2NP
- [^{48}V]TiO_2NP accumulation and retention in secondary organs and tissues relative to the entire translocated fraction through ABB
- Determination of fast mucociliary nanoparticle clearance from airways and macrophage-mediated long-term nanoparticle clearance from the peripheral lungs
- Differentiation of [^{48}V]TiO_2NP translocated across the ABB *versus* [^{48}V]TiO_2NP absorbed across the GIT walls
- [^{48}V]TiO_2NP relocation within the lungs
- [^{48}V]TiO_2NP in the trachea and main bronchi
- Estimated hepato-biliary clearance (HBC) of [^{48}V]TiO_2NP

References

Abbas, K, Cydzik, I, Del Torchio, R, Farina, M, Forti, E, Gibson, N, Holzwarth, U, Simonelli, F & Kreyling, W 2010. Radiolabelling of TiO2 nanoparticles for radiotracer studies. *Journal of Nanoparticle Research,* 12**,** 2435-2443.

Almeida, JPM, Chen, AL, Foster, A & Drezek, R 2011. In vivo biodistribution of nanoparticles. *Nanomedicine,* 6**,** 815-835.

Baan, RA 2007. Carcinogenic Hazards from Inhaled Carbon Black, Titanium Dioxide, and Talc not Containing Asbestos or Asbestiform Fibers: Recent Evaluations by an IARC Monographs Working Group. *Inhalation Toxicology,* 19**,** 213-228.

Baisch, BL, Corson, NM, Wade-Mercer, P, Gelein, R, Kennell, AJ, Oberdorster, G & Elder, A 2014. Equivalent titanium dioxide nanoparticle deposition by intratracheal instillation and whole body inhalation: the effect of dose rate on acute respiratory tract inflammation. *Part Fibre Toxicol,* 11**,** 5.

Christensen, FM, Johnston, HJ, Stone, V, Aitken, RJ, Hankin, S, Peters, S & Aschberger, K 2011. Nano-TiO(2) - feasibility and challenges for human health risk assessment based on open literature. *Nanotoxicology,* 5**,** 110-24.

Echa-Corap 2016. Community rolling action plan (CoRAP) update covering years 2014, 2015 and 2016 of the European Chemicals Agency, European Commission. *Available on: http://echa.europa.eu/documents/10162/13628/corap_list_2014-2016_en.pdf,* Accessed on April 04, 2016.

Ferin, J, Oberdorster, G & Penney, DP 1992. Pulmonary retention of ultrafine and fine particles in rats. *Am J Respir Cell Mol Biol,* 6**,** 535-42.

Fromen, CA, Rahhal, TB, Robbins, GR, Kai, MP, Shen, TW, Luft, JC & Desimone, JM 2016. Nanoparticle surface charge impacts distribution, uptake and lymph node trafficking by pulmonary antigen-presenting cells. *Nanomedicine,* 12**,** 677-87.

Geiser, M, Casaulta, M, Kupferschmid, B, Schulz, H, Semmler-Behnke, M & Kreyling, W 2008. The role of macrophages in the clearance of inhaled ultrafine titanium dioxide particles. *American Journal of Respiratory Cell and Molecular Biology,* 38**,** 371-6.

Geiser, M & Kreyling, WG 2010. Deposition and biokinetics of inhaled nanoparticles. *Part Fibre Toxicol,* 7**,** 2.

Geiser, M, Rothen-Rutishauser, B, Kapp, N, Schurch, S, Kreyling, W, Schulz, H, Semmler, M, Im Hof, V, Heyder, J & Gehr, P 2005. Ultrafine particles cross cellular membranes by nonphagocytic mechanisms in lungs and in cultured cells. *Environmental Health Perspectives,* 113**,** 1555-60.

Gibson, N, Holzwarth, U, Abbas, K, Simonelli, F, Kozempel, J, Cydzik, I, Cotogno, G, Bulgheroni, A, Gilliland, D, Ponti, J, Franchini, F, Marmorato, P, Stamm, H, Kreyling, W, Wenk, A, Semmler-Behnke, M, Buono, S, Maciocco, L & Burgio, N 2011. Radiolabelling of engineered nanoparticles for in vitro and in vivo tracing applications using cyclotron accelerators. *Archives of Toxicology,* 85**,** 751-73.

Hildebrand, H, Schymura, S, Holzwarth, U, Gibson, N, Dalmiglio, M & Franke, K 2015. Strategies for radiolabeling of commercial TiO2 nanopowder as a tool for sensitive nanoparticle detection in complex matrices. *Journal of Nanoparticle Research,* 17**,** 1-12.

Hirn, S, Semmler-Behnke, M, Schleh, C, Wenk, A, Lipka, J, Schaffler, M, Takenaka, S, Moller, W, Schmid, G, Simon, U & Kreyling, WG 2011. Particle size-dependent and surface charge-dependent biodistribution of gold nanoparticles after intravenous administration. *European Journal of Pharmaceutics and Biopharmaceutics,* 77**,** 407-16.

Holzwarth, U, Bulgheroni, A, Gibson, N, Kozempel, J, Cotogno, G, Abbas, K, Simonelli, F & Cydzik, I 2012. Radiolabelling of nanoparticles by proton irradiation: temperature control in nanoparticulate powder targets. *Journal of Nanoparticle Research,* 14.

Kreyling, W & Scheuch, G 2000. Clearance of particles deposited in the lungs. *In:* Heyder, J & Gehr, P (eds.) *Particle Lung Interactions.* New York, USA: Marcel Dekker.

Kreyling, WG 1990. Interspecies comparison of lung clearance of "insoluble" particles. *Journal of Aerosol Medicine,* 3**,** S93-S110.

Kreyling, WG, Abdelmonem, AM, Ali, Z, Alves, F, Geiser, M, Haberl, N, Hartmann, R, Hirn, S, De Aberasturi, DJ, Kantner, K, Khadem-Saba, G, Montenegro, J-M, Rejman, J, Rojo, T, De Larramendi, IR, Ufartes, R, Wenk, A & Parak, WJ 2015. In vivo integrity of polymer-coated gold nanoparticles. *Nat Nano,* advance online publication.

Kreyling, WG, Biswas, P, Messing, ME, Gibson, N, Geiser, M, Wenk, A, Sahu, M, Deppert, K, Cydzik, I, Wigge, C, Schmid, O & Semmler-Behnke, M 2011. Generation and characterization of stable, highly concentrated titanium dioxide nanoparticle aerosols for rodent inhalation studies. *Journal of Nanoparticle Research,* 13**,** 511–524.

Kreyling, WG, Hirn, S, Moller, W, Schleh, C, Wenk, A, Celik, G, Lipka, J, Schaffler, M, Haberl, N, Johnston, BD, Sperling, R, Schmid, G, Simon, U, Parak, WJ & Semmler-Behnke, M 2014. Air-blood barrier translocation of tracheally instilled gold nanoparticles inversely depends on particle size. *ACS Nano,* 8**,** 222-33.

Kreyling, WG, Holzwarth, U, Haberl, N, Kozempel, J, Wenk, A, Hirn, S, Schleh, C, Schäffler, M, Lipka, J, Semmler-Behnke, M & Gibson, N submitted-a. Part 1: Quantitative biokinetics of titanium dioxide nanoparticles after intravenous injection in rats *Nanotoxicology***,** (submitted).

Kreyling, WG, Holzwarth, U, Schleh, C, Kozempel, J, Wenk, A, Haberl, N, Hirn, S, Schäffler, M, Lipka, J, Semmler-Behnke, M & Gibson, N submitted-b. Part 2: Quantitative biokinetics of titanium dioxide nanoparticles after oral application in rats *Nanotoxicology***,** (submitted).

Kreyling, WG, Semmler-Behnke, M, Seitz, J, Scymczak, W, Wenk, A, Mayer, P, Takenaka, S & Oberdorster, G 2009. Size dependence of the translocation of inhaled iridium and carbon nanoparticle aggregates from the lung of rats to the blood and secondary target organs. *Inhalation Toxicology,* 21**,** 55-60.

Kreyling, WG, Semmler-Behnke, M, Takenaka, S & Moller, W 2013. Differences in the biokinetics of inhaled nano- versus micrometer-sized particles. *Acc Chem Res,* 46**,** 714-22.

Kreyling, WG, Semmler, M, Erbe, F, Mayer, P, Takenaka, S, Schulz, H, Oberdörster, G & Ziesenis, A 2002. Translocation of ultrafine insoluble iridium particles from lung epithelium to extrapulmonary organs is size dependent but very low. *Journal of Toxicology and Environmental Health-Part A,* 65**,** 1513-1530.

Lehnert, BE, Valdez, YE & Tietjen, GL 1989. Alveolar macrophage-particle relationships during lung clearance. *Am J Respir Cell Mol Biol,* 1**,** 145-54.

Milani, S, Bombelli, FB, Pitek, AS, Dawson, KA & Radler, J 2012. Reversible versus irreversible binding of transferrin to polystyrene nanoparticles: soft and hard corona. *ACS Nano,* 6**,** 2532-41.

Niosh 2011. Occupational Exposure to Titanium Dioxide. *NIOSH CURRENT INTELLIGENCE BULLETIN 63,* NIOSH Publication No.160**,** 1-140.

Oeff, K & Konig, A 1955. [Blood volume of rat organs and residual amount of blood after blood letting or irrigation; determination with radiophosphorus-labeled erythrocytes.]. *Naunyn-Schmiedebergs Archiv für Experimentelle Pathologie und Pharmakologie,* 226**,** 98-102.

Schäffler, M, Sousa, F, Wenk, A, Sitia, L, Hirn, S, Schleh, C, Haberl, N, Violatto, M, Canovi, M, Andreozzi, P, Salmona, M, Bigini, P, Kreyling, WG & Krol, S 2014. Blood protein coating of gold nanoparticles as potential tool for organ targeting. *Biomaterials,* 35**,** 3455-66.

Schleh, C, Semmler-Behnke, M, Lipka, J, Wenk, A, Hirn, S, Schaffler, M, Schmid, G, Simon, U & Kreyling, WG 2012. Size and surface charge of gold nanoparticles determine absorption across intestinal barriers and accumulation in secondary target organs after oral administration. *Nanotoxicology,* 6**,** 36-46.

Semmler-Behnke, M, Takenaka, S, Fertsch, S, Wenk, A, Seitz, J, Mayer, P, Oberdorster, G & Kreyling, WG 2007. Efficient elimination of inhaled nanoparticles from the alveolar region: evidence for interstitial uptake and subsequent reentrainment onto airways epithelium. *Environmental Health Perspectives,* 115**,** 728-33.

Semmler, M, Seitz, J, Erbe, F, Mayer, P, Heyder, J, Oberdorster, G & Kreyling, WG 2004. Long-term clearance kinetics of inhaled ultrafine insoluble iridium particles from the rat lung, including transient translocation into secondary organs. *Inhalation Toxicology,* 16**,** 453-9.

669 Shi, H, Magaye, R, Castranova, V & Zhao, J 2013. Titanium dioxide nanoparticles: a review of current
670 toxicological data. *Part Fibre Toxicol,* 10**,** 15.
671 Stone, KC, Mercer, RR, Gehr, P, Stockstill, B & Crapo, JD 1992. Allometric relationships of cell
672 numbers and size in the mammalian lung. *American Journal of Respiratory Cell and Molecular*
673 *Biology,* 6**,** 235-43.
674 Vogelsberger, W, Schmidt, J., Roelfs, F. 2008. Dissolution kinetics of oxide nanoparticles: The
675 observation of an unusual behaviour. . *Colloids and Surfaces A,* 324**,** 51-57.
676
677

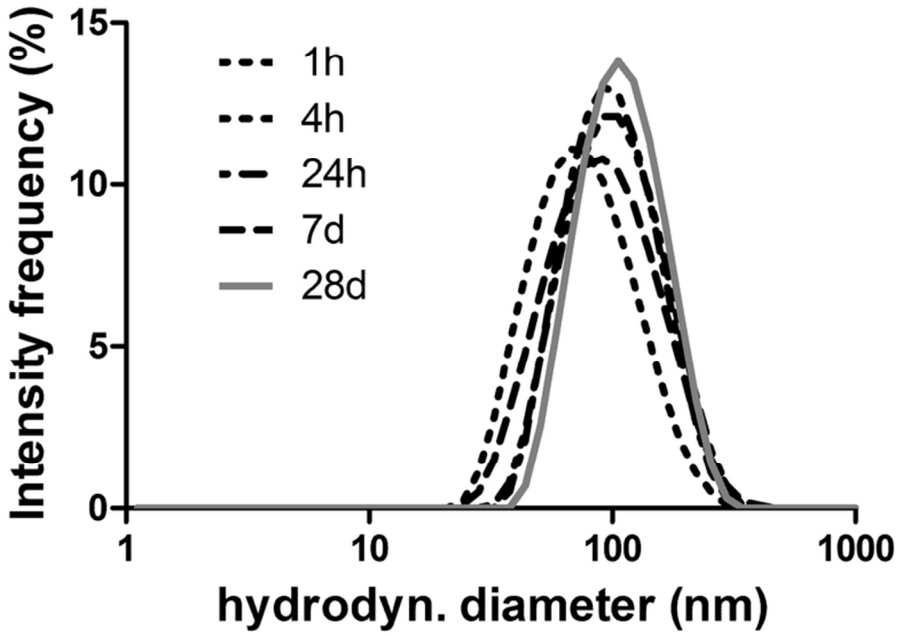

Figure 1: Hydrodynamic diameter of the five separately prepared [48V]TiO2NP suspensions used to study the retention time-points 1h, 4h, 24h, 7d; and 28d, measured directly before application.

73x52mm (300 x 300 DPI)

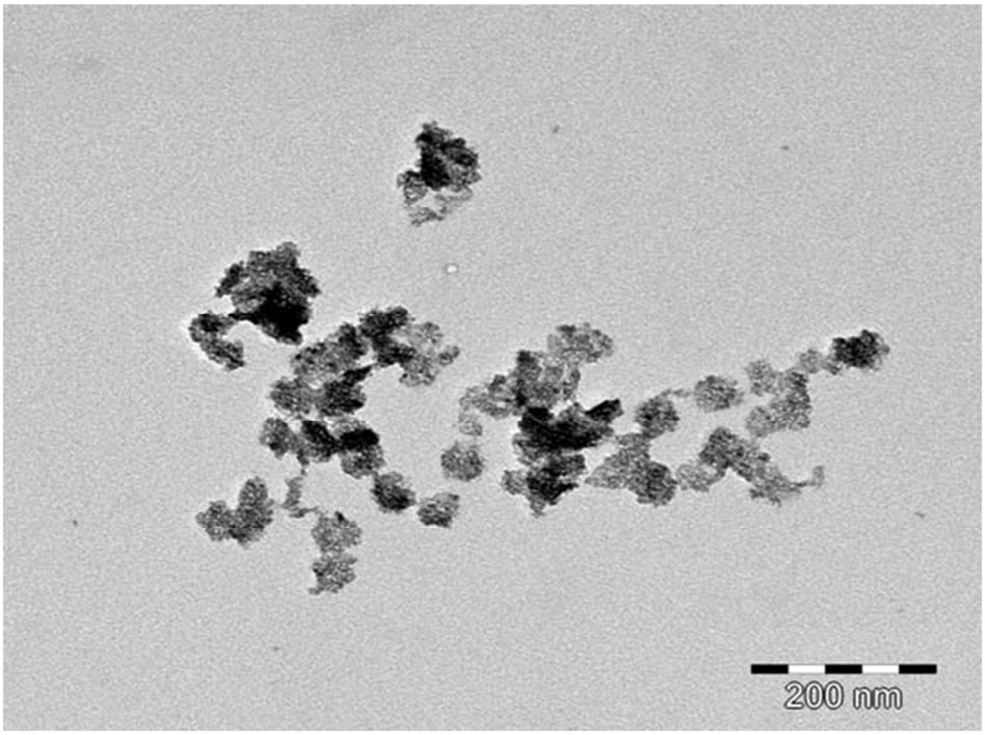

Figure 2: Transmission electron micrograph of size-selected TiO2NP sampled immediately after the size-selection procedure. Sample preparation leads to 'clumping' of aggregates/agglomerates on the support grid.

254x190mm (96 x 96 DPI)

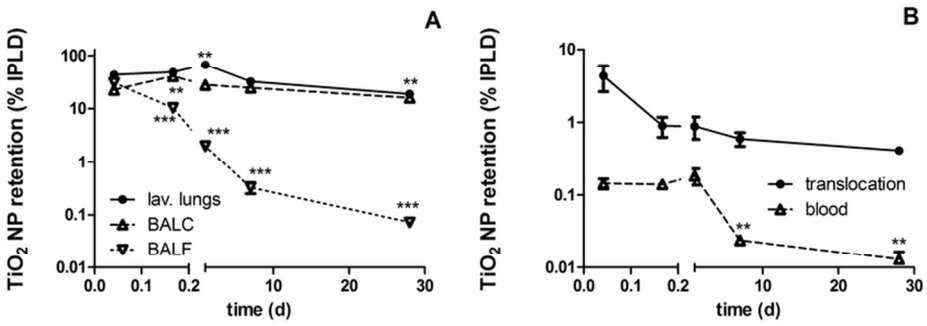

Figure 3: A: [48V]TiO2NP retention in lavaged lungs, in BALC and in BALF. Data are given as fractions of IPLD. B: kinetics of total [48V]TiO2NP translocation across the ABB and [48V]TiO2NP content in total blood relative to the IPLD. Data are corrected for [48V]TiO2NP retained in the residual blood volume of organs and tissues. Mean ± SEM of n=4 rats at each time point. Significant difference from [48V]TiO2NP retention at 1h: $p<0.01$ (**);$p<0.001$ (***).

77x28mm (300 x 300 DPI)

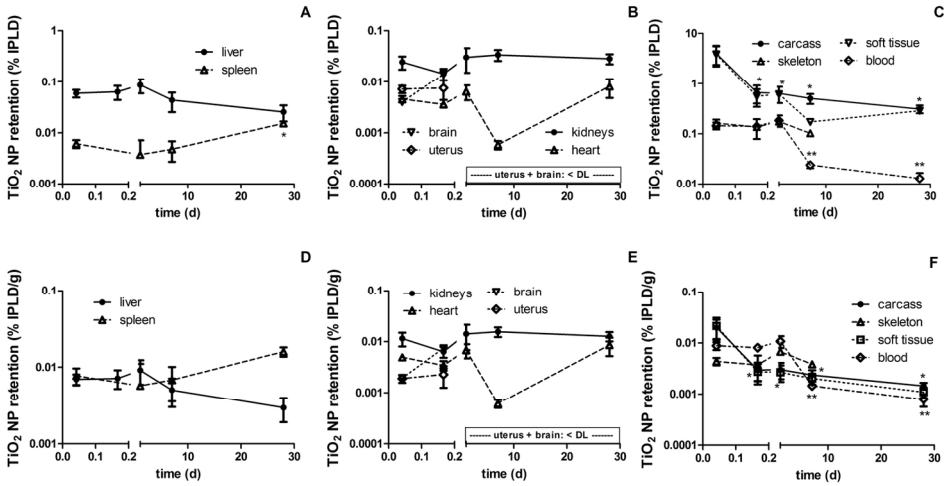

Figure 4: Nanoparticle retention (from Table 3) in percent of IPLD after IT-instillation visualized for liver and spleen (panel A), kidneys, heart, brain and uterus (panel B), and blood and carcass (subdivided into skeleton and soft tissues) (panel C). Panels D to E show the corresponding values normalized to the mass of the organs or tissues as %IPLD•g-1. Mean ± SEM of n=4 rats at each time point. Significant difference from [48V]TiO2NP retention at 1h: $p<0.05$ (*), $p<0.01$ (**).

149x79mm (300 x 300 DPI)

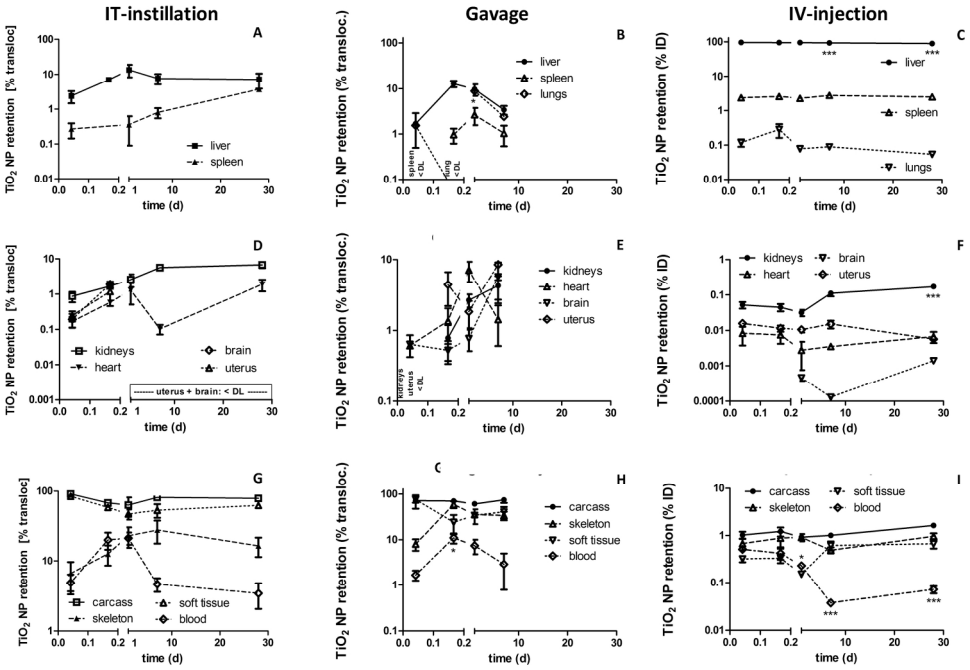

Figure 5: Comparison of the biokinetics of [48V]TiO2NP translocated across the ABB after intratracheal instillation with the biokinetics of [48V]TiO2NP absorbed across the gut walls after gavage (Kreyling, submitted-b) and with [48V]TiO2NP after IV-injection (Kreyling, submitted-a). Gavage data were only collected for one week after administration. Mean ± SEM of n=4 rats at each time point. Significant difference from [48V]TiO2NP retention at 1h: $p<0.05$ (*); $p<0.01$ (**); $p<0.001$ (***).

188x132mm (300 x 300 DPI)

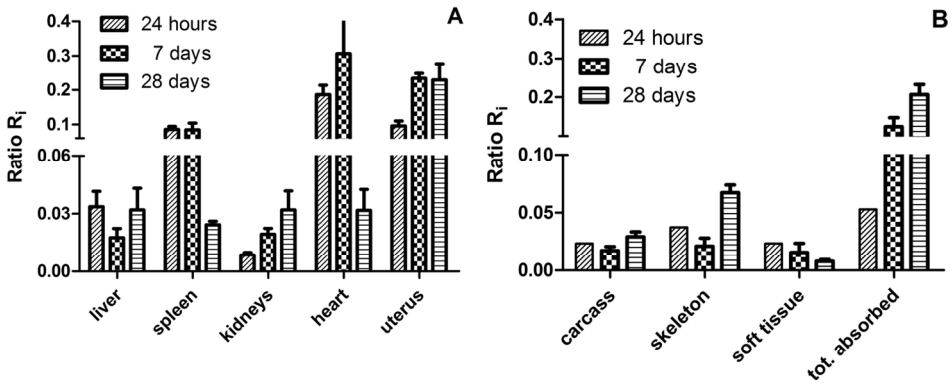

Figure 6: The ratios Ri represent the fractions of [48V]TiO2NP present in an organ or tissue after IT-instillation that has been absorbed through the GIT relative to the sum of gut-absorbed and ABB-translocated [48V]TiO2NP after days 1, 7 and 28; panel A: for individual secondary organs, panel B: for carcass (subdivided into skeleton and soft tissues) and total translocation. Mean ± SEM of n=4 rats at each time point.

133x62mm (300 x 300 DPI)

Table 1: Physicochemical characteristics of the [^{48}V]TiO_2NP suspensions used for IT-instillation studies at five different retention times and the mean values of the applied ^{48}V activity and mass of [^{48}V]TiO_2NP effectively received by the rats. The mean dose in µg/kg BW is also given. Additionally, [^{48}V]TiO_2NP losses in the syringe and/or cannula are provided as detailed in SI-IT.

Retention time		1h	4h	24h	7d	28d
Zeta Potential	[mV]	-38.9 ± 4.2	-33.2 ± 2.4	-29.9 ± 8.1	-42.7 ± 9.2	-35.2 ± 7.6
Z-average	[nm]	93	72	93	82	101
PDI		0.157	0.228	0.160	0.197	0.135
Effective ^{48}V radioactivity received by rats (ID)	[kBq]	11.7 ± 1.6	10.9 ± 1.0	11.1 ± 1.3	145.8 ± 44.1	47.8 ± 9.2
Applied [^{48}V]TiO_2NP mass	[µg]	11.7 ± 1.6	10.9 ± 1.0	11.1 ± 1.3	62.1 ± 18.7	20.3 ± 3.9
Applied [^{48}V]TiO_2NP dose	[µg•kg^{-1} BW]	44.7 ± 6.7	39.6 ± 3.3	41.1 ± 3.7	238.4 ± 74.6	77.6 ± 14.9
Effective ^{48}V radio-activity in peripheral lungs (IPLD)	[kBq]	8.4 ± 1.7	7.4 ± 1.2	8.4 ± 1	90.1 ± 27	24.5 ± 12.2
Percentage of [^{48}V]TiO_2NP retained in the syringe after application		51 ± 14 %	38 ± 6 %	13 ± 4 %	n.d.	n.d.

Table 2: Fast [^{48}V]TiO_2NP mucociliary clearance (during the first two days) and long-term macrophage-mediated clearance of [^{48}V]TiO_2NP (from day 3-28 after IT-instillation) as percentages of the effectively instilled dose (calculation see SM-IT).

Retention time-point	Fast mucociliary cleared fraction (mean±SEM)	Long-term macrophage-mediated cleared fraction (mean±SEM)
1h	30.9±4.9 %	
4h	31.9±5.8 %	
24h	28.7±5.5 %	
7d	36.4±14.6 %	26.0±8.1 %
28d	49.6±21.6 %	30.5±13.2 %

Table 3: [^{48}V]TiO_2NP retention in organs and tissues 1h, 4 h, 24h, 7d and 28d after intratracheal instillation. The raw data are presented as retained percentage of the IPLD of [^{48}V]TiO_2NP (corrected for decay). The raw data were corrected for the [^{48}V]TiO_2NP content in residual blood after exsanguination (w/o residual blood content) and additionally for the contributions of free ^{48}V-ions (w/o free ^{48}V). After these corrections the ^{48}V-activity data were converted into [^{48}V]TiO_2NP concentrations per mass of organ or tissue, given in ng·g^{-1} and as % IPLD·g^{-1}. Since the applied [^{48}V]TiO_2NP doses exhibited a scatter and were intentionally increased for the 7d and 28d groups most mass concentrations in ng·g^{-1} exhibit an increase from 24h to 7d. The values in % IPLD·g^{-1} are independent of the exactly applied doses. The sixth line for each organ presents the distribution of those [^{48}V]TiO_2NP that passed the ABB (% translocated TiO_2). (< DL = below detection limit). In the last line "% translocated TiO_2" the [^{48}V]TiO_2NP fractions were normalized to those [^{48}V]TiO_2NP which had crossed the ABB and entered blood circulation; see Supp-IT.

organ	retention time (d) percent (%)	1h mean ± SEM	4h mean ± SEM	24h mean ± SEM	7d mean ± SEM	28d mean ± SEM
lungs+BAL	raw data (%IPLD)	95.61 ± 1.66	98.72 ± 0.23	96.84 ± 0.40	64.69 ± 2.07	44.49 ± 0.72
lungs+BAL	w/o resid. blood cont.	95.61 ± 1.66	98.71 ± 0.23	96.83 ± 0.40	56.80 ± 3.72	34.62 ± 1.05
lungs+BAL	w/o free ^{48}V	95.60 ± 1.66	98.68 ± 0.23	98.94 ± 0.39	56.74 ± 3.72	34.55 ± 1.06
lungs+BAL	TiO_2 conc. (% IPLD/g tiss.)	25.10 ± 0.23	23.58 ± 1.79	23.48 ± 1.56	13.68 ± 1.23	8.96 ± 0.58
lungs+BAL	TiO_2 conc. (ng/g tiss.)	2108.6 ± 232.8	1744.3 ± 161.8	1976.7 ± 194.2	3435.3 ± 1097.3	363.6 ± 88.4
lungs+BAL	no translocation					
lungs	raw data (%IPLD)	42.85 ± 4.21	48.13 ± 0.78	66.98 ± 5.12	36.36 ± 3.30	24.05 ± 1.92
lungs	w/o resid. blood cont.	42.84 ± 4.21	48.12 ± 0.78	66.97 ± 5.12	32.00 ± 3.70	18.74 ± 1.65
lungs	w/o free ^{48}V	42.83 ± 4.21	48.09 ± 0.78	68.38 ± 5.33	31.95 ± 3.71	18.67 ± 1.65
lungs	TiO_2 conc. (% IPLD/g tiss.)	12.57 ± 1.20	12.77 ± 1.23	18.08 ± 2.3	8.62 ± 1.29	5.45 ± 0.68
lungs	TiO_2 conc. (ng/g tiss.)	1073 ± 194	941 ± 90	1543 ± 278.	2229 ± 799	218 ± 59
lungs	no translocation					

liver	raw data (%IPLD)	0.074 ± 0.009	0.087 ± 0.016	0.163 ± 0.015	0.110 ± 0.021	0.099 ± 0.008
liver	w/o resid. blood cont.	0.063 ± 0.010	0.076 ± 0.017	0.142 ± 0.011	0.094 ± 0.019	0.075 ± 0.006
liver	w/o free ^{48}V	0.060 ± 0.010	0.064 ± 0.020	0.088 ± 0.023	0.043 ± 0.015	0.026 ± 0.008
liver	TiO_2 conc. (% IPLD/g tiss.)	0.007 ± 0.001	0.007 ± 0.002	0.009 ± 0.003	0.005 ± 0.002	0.003 ± 0.001
liver	TiO_2 conc. (ng/g tiss.)	0.57 ± 0.07	0.52 ± 0.13	0.74 ± 0.17	1.03 ± 0.24	0.15 ± 0.05
liver	% translocated TiO_2	2.39 ± 1.84	7.03 ± 1.97	13.6 ± 9.2	7.72 ± 5.06	7.23 ± 5.80
spleen	raw data (%IPLD)	0.008 ± 0.0009	no data	0.010 ± 0.001	0.014 ± 0.002	0.031 ± 0.005
spleen	w/o resid. blood cont.	0.006 ± 0.001	no data	0.009 ± 0.001	0.012 ± 0.002	0.024 ± 0.003
spleen	w/o free ^{48}V	0.006 ± 0.001	no data	0.004 ± 0.003	0.005 ± 0.002	0.015 ± 0.001
spleen	TiO_2 conc. (% IPLD/g tiss.)	0.008 ± 0.002	no data	0.006 ± 0.005	0.007 ± 0.003	0.016 ± 0.002
spleen	TiO_2 conc. (ng/g tiss.)	0.61 ± 0.11	no data	0.42 ± 0.33	1.20 ± 0.20	0.66 ± 0.17
spleen	% translocated TiO_2	0.27± 0.25	no data	0.36 ± 0.47	0.81 ± 0.52	3.73 ± 0.42
kidneys	raw data (%IPLD)	0.033 ± 0.006	0.033 ± 0.003	0.109 ± 0.011	0.081 ± 0.009	0.096 ± 0.013
kidneys	w/o resid. blood cont.	0.029 ± 0.006	0.0280 ± 0.003	0.102 ± 0.010	0.071 ± 0.009	0.074 ± 0.010
kidneys	w/o free ^{48}V	0.025 ± 0.007	0.015 ± 0.004	0.031 ± 0.013	0.033 ± 0.007	0.029 ± 0.006
kidneys	TiO_2 conc. (% IPLD/g tiss.)	0.012 ± 0.004	0.004 ± 0.002	0.014 ± 0.006	0.016 ± 0.003	0.013 ± 0.003
kidneys	TiO_2 conc. (ng/g tiss.)	0.89 ± 0.20	0.46 ± 0.10	1.12 ± 0.47	3.38 ± 0.65	0.54 ± 0.18
kidneys	% translocated TiO_2	0.87 ± 0.56	1.70 ± 0.34	2.6 ± 1.79	5.70 ± 1.45	6.81 ± 2.58
heart	raw data (%IPLD)	0.006 ± 0.0007	0.005 ± 0.0008	0.012 ± 0.002	0.002 ± 0.0001	0.013 ± 0.005
heart	w/o resid. blood cont.	0.005 ± 0.0006	0.004 ± 0.0007	0.010 ± 0.001	0.002 ± 0.0001	0.010 ± 0.004
heart	w/o free ^{48}V	0.005 ± 0.0007	0.003 ± 0.0006	0.007 ± 0.002	0.0006 ± 0.0002	0.008 ± 0.003
heart	TiO_2 conc. (% IPLD/g tiss.)	0.005 ± 0.0005	0.003 ± 0.0007	0.007 ± 0.0022	0.0006 ± 0.0002	0.009 ± 0.003
heart	TiO_2 conc. (ng/g tiss.)	0.40 ± 0.018	0.25 ± 0.04	0.58 ± 0.18	0.14 ± 0.04	0.25 ± 0.07
heart	% translocated TiO_2	0.17 ± 0.117	0.58 ± 0.11	1.29 ± 1.56	0.10 ± 0.06	1.90 ± 1.41
brain	raw data (%IPLD)	0.005 ± 0.001	0.015 ± 0.0006	0.001 ± 0.0005	0.001 ± 0.001	< DL
brain	w/o resid. blood cont.	0.005 ± 0.0012	0.014 ± 0.0006	< DL	0.001 ± 0.001	< DL
brain	w/o free ^{48}V	0.004 ± 0.0004	0.014 ± 0.0006	< DL	< DL	< DL
brain	TiO_2 conc. (% IPLD/g tiss.)	0.002 ± 0.0002	0.007 ± 0.0002	< DL	< DL	< DL
brain	TiO_2 conc. (ng/g tiss.)	0.15 ± 0.02	0.55 ± 0.0296	< DL	< DL	< DL

brain	% translocated TiO_2	0.19 ± 0.14	1.91 ± 0.76	< DL	< DL	< DL
uterus	raw data (%IPLD)	0.008 ± 0.001	0.010 ± 0.003	0.007 ± 0.0008	0.006 ± 0.0007	0.007 ± 0.001
uterus	w/o resid. blood cont.	0.008 ± 0.001	0.009 ± 0.003	0.006 ± 0.0008	0.005 ± 0.0007	0.005 ± 0.001
uterus	w/o free ^{48}V	0.007 ± 0.001	0.008 ± 0.003	< DL	< DL	< DL
uterus	TiO_2 conc. (% IPLD/g tiss.)	0.002 ± 0.0003	0.002 ± 0.001	< DL	< DL	< DL
uterus	TiO_2 conc. (ng/g tiss.)	0.157 ± 0.025	0.174 ± 0.088	< DL	< DL	< DL
uterus	% translocated TiO_2	0.25 ± 0.16	1.18 ± 1.44	< DL	< DL	< DL
carcass	raw data (%IPLD)	4.13 ± 1.66	0.85 ± 0.23	1.48 ± 0.25	1.23 ± 0.11	1.20 ± 0.12
carcass	w/o resid. blood cont.	4.09 ± 1.66	0.82 ± 0.23	1.41 ± 0.24	1.08 ± 0.12	0.92 ± 0.09
carcass	w/o free ^{48}V	4.05 ± 1.66	0.66 ± 0.26	0.65 ± 0.23	0.49 ± 0.12	0.31 ± 0.05
carcass	TiO_2 conc. (% IPLD/g tiss.)	0.02 ± 0.009	0.003 ± 0.001	0.003 ± 0.001	0.002 ± 0.0006	0.002 ± 0.0002
carcass	TiO_2 conc. (ng/g tiss.)	1.79 ± 0.84	0.21 ± 0.08	0.34 ± 0.05	0.54 ± 0.16	0.062 ± 0.016
carcass	% translocated TiO_2	91.06 ± 5.93	67.763± 12.78	63.24 ± 36.16	80.97 ± 7.92	78.68 ± 7.78
blood	raw data (%IPLD)	0.150 ± 0.022	0.159 ± 0.013	0.262 ± 0.040	0.037 ± 0.004	0.029 ± 0.005
blood	w/o resid. blood cont.	0.150 ± 0.022	0.159 ± 0.013	0.262 ± 0.040	0.037 ± 0.004	0.029 ± 0.005
blood	w/o free ^{48}V	0.144 ± 0.023	0.140 ± 0.009	0.187 ± 0.042	0.024 ± 0.003	0.013 ± 0.004
blood	TiO_2 conc. (% IPLD/g tiss.)	0.009 ± 0.002	0.008 ± 0.0005	0.011 ± 0.003	0.001 ± 0.0002	0.001 ± 0.0002
blood	TiO_2 conc. (ng/g tiss.)	1.24 ± 0.26	0.61 ± 0.07	0.89 ± 0.19	0.347 ± 0.10	0.034 ± 0.016
blood	% translocated TiO_2	4.84 ± 3.07	19.96 ± 10.96	21.26 ± 7.38	4.61 ± 2.03	3.40 ± 2.70
skeleton	raw data (%IPLD)	0.205 ± 0.027	0.209 ± 0.057	0.501 ± 0.069	0.425 ± 0.075	0.426 ± 0.068
skeleton	w/o resid. blood cont.	0.191 ± 0.029	0.194 ± 0.057	0.476 ± 0.069	0.343 ± 0.052	0.181 ± 0.057
skeleton	w/o free ^{48}V	0.161 ± 0.030	0.118 ± 0.045	0.284 ± 0.067	0.137 ± 0.021	0.072 ± 0.023
skeleton	TiO_2 conc. (% IPLD/g tiss.)	0.004 ± 0.0007	0.004 ± 0.002	0.011 ± 0.003	0.005 ± 0.001	0.003 ± 0.001
skeleton	TiO_2 conc. (ng/g tiss.)	0.50 ± 0.07	0.30 ± 0.11	0.89 ± 0.23	0.46 ± 0.19	0.09 ± 0.03
skeleton	% translocated TiO_2	6.62 ± 5.97	12.60 ± 7.00	22.88 ± 12.94	27.71 ± 20.07	16.46 ± 10.22
soft tissue	raw data (%IPLD)	3.920 ± 1.675	0.644 ± 0.200	0.983 ± 0.201	0.809 ± 0.138	0.774 ± 0.058
soft tissue	w/o resid. blood cont.	3.892 ± 1.67	0.613 ± 0.203	0.938 ± 0.195	0.735 ± 0.140	0.744 ± 0.042
soft tissue	w/o free ^{48}V	3.885 ± 1.673	0.544 ± 0.221	0.579 ± 0.208	0.423 ± 0.108	0.249 ± 0.044
soft tissue	TiO_2 conc. (% IPLD/g tiss.)	0.022 ± 0.010	0.003 ± 0.001	0.003 ± 0.001	0.002 ± 0.0005	0.001 ± 0.0002

soft tissue	TiO_2 conc. (ng/g tiss.)	1.77 ± 0.87	0.145 ± 0.110	0.302 ± 0.049	0.460 ± 0.138	0.054 ± 0.012
soft tissue	% translocated TiO_2	84.44 ± 11.73	55.12 ± 9.86	40.34 ± 13.46	53.27 ± 23.26	62.22 ± 7.45

- No correction "w/o resid. blood cont." was calculated for blood.
- The mass of "lungs+BAL" is calculated to be the sum of the lavaged lung weight plus the estimated masses of BAL cells and BAL fluid: Volume of BAL cells are estimated using a mean alveolar macrophage volume of $6.4 \cdot 10^{-10}$ cm³ (Stone et al., 1992) times in average $4 \cdot 10^{6}$ lavaged AM ➔ 0.0025 cm³; assuming unit density the lavaged cell mass is 0.0025 g.
- Volume of BAL fluid is estimated using the rat alveolar surface area of 0.40 m² (Stone et al., 1992) times an assumed epithelial lining fluid (ELF) thickness of 2 µm ➔ 0.8 cm³; assuming ELF harvesting efficiency during BAL of 50% and unit density the BAL fluid mass is 0.4 g.